UV-induced porosity using photogenerated acids to catalyze the decomposition of sacrificial polymers templated in dielectric films

Jassem Abdallah, Marshall Silver,† Sue Ann Bidstrup Allen and Paul A. Kohl*

Received 8th May 2006, Accepted 16th November 2006
First published as an Advance Article on the web 8th December 2006
DOI: 10.1039/b606438h

A UV-initiated process for selective incorporation of porosity and tuning of refractive index in a dielectric film is presented. The formation of porosity *via* radiation offers the advantages of lower processing temperatures and shorter processing times than most processes that rely on thermally-induced porosity. The ability to pattern porosity *via* the use of a photomask allows structures such as porous direct-write waveguides to be made. The direct-write process presented here used UV-generated acids to catalyze the decomposition of sacrificial polymers templated in a crosslinked matrix, resulting in the formation of porosity and decrease of refractive index and dielectric constant after subsequent removal of the generated acid. In unexposed areas, no acid molecules were generated, thus these areas remained non-porous and their refractive index remained relatively high compared to porous regions. Base-catalyzed gelation was used to crosslink the matrix at temperatures well below the glass transition temperature of the matrix in order to avoid thermal activation of the photoacid generators (PAGs) in the direct-write formulation. After crosslinking the matrix, deep ultraviolet (DUV) radiation was used to initiate the direct-write reactions thus creating a refractive index profile within the film. Neutralization or volatilization of the photogenerated acid was used to deactivate the system. The lowest interline dielectric constant achieved by direct-written films was 2.36 after the volatilization step compared to a value of 2.29 for porous films formed *via* the traditional template process. At optimum conditions, the average amount of UV-induced porosity was estimated to be as high as 21%. Transmission electron microscopy (TEM) imaging showed that elongated mesopores (10 nm by about 20–30 nm) and elongated macropores (100 nm by about 200 nm in size) were produced within the internal structure of direct-written films. The porous films formed *via* the traditional template technique had internal structures with large collections of spherical mesopores (5–10 nm) located in close proximity to one another due to phase segregation of the polymer at high temperatures.

Introduction

The incorporation of porosity in a material potentially results in the lowering of its dielectric constant, the enhancement of its flexibility and crack-resistance, and the lowering of its refractive index and has generated much interest both in academia and in the microelectronics industry.[1–22] The final physical properties of porous films are dependent on the final pore structure characteristics, such as the total amount of porosity; the pore sizes and pore size distribution; the presence or absence of pore interconnectivity, among other parameters.[1–4,6,7,9,16–19,22–24] The differences in the morphologies of the final pore structures result from variations in physical conditions used when fabricating porous films; important factors include the type of porogen (thermally decomposable polymer or volatile solvent) used, the porogen loading, the presence or absence of phase segregation of porogen during processing, the processing temperatures required, and other physical conditions.[2,6,9,23] The traditional template technique for fabricating a porous thin film makes use of a porogen distributed in a crosslinkable matrix.[2] During processing, the matrix is cured to instill mechanical integrity, before the film is heated to high temperatures to decompose and volatilize the templated polymer. As the decomposition by-products diffuse out of the films, air diffuses in to replace the porogen, resulting in the formation of air pockets in place of the sacrificial polymer chains. The total processing time for the template technique may be several hours because of the necessity of thermally setting the matrix as well as decomposing the polymer *via* a slow ramp in temperature to the decomposition point of the porogen and a dwell time to ensure the removal of all of the porogen.[2–8] Additionally films must be allowed to cool slowly prior to removal from furnaces otherwise there will be formation of cracks due to internal stress resulting from the thermal shock of exposing the very hot films to ambient conditions. An additional disadvantage of thermally decomposing a porogen to produce porosity is that many organic materials cannot be used as substrates owing to their degradation at the high temperatures required to decompose the templated polymers. Finally, the high temperatures required to thermally decompose polymers encourage phase segregation and agglomeration of the macromolecules prior

School of Chemical and Biomolecular Engineering, Georgia Institute of Technology, Atlanta, GA, 30332, USA.
E-mail: paul.kohl@che.gatech.edu; Fax: +1-404-894-2866;
Tel: +1-404-894-2893
† Present address: Department of Chemical Engineering, The University of Texas at Austin, Austin, TX 78712, USA.

to decomposition thus producing large, non-uniformly dispersed pores that may produce undesirable final properties in the porous films.[6,7]

The development of a direct-write method for producing porosity whereby photodefinable polymers are either directly or indirectly decomposed *via* radiation would decrease the temperature required to decompose the polymer chains and may also lead to a decrease in the overall processing time. The lower temperatures may potentially allow organic substrates to be used as well as reduce the tendency for polymers to phase segregate during the procedure. Furthermore, UV-induced decomposition enables the lateral patterning of porosity, which may be used to make interesting devices in which functionality is dependent on the level of porosity present (*e.g.* phase masks, or lateral confinement in waveguides due to a refractive index profile).[25,26] Recently, researchers have made use of the photocleavable nature of Si–Si bonds in the structure of polysilanes to UV-induce porosity in hybrid films composed of methacrylate–polysilane copolymers (MPS) chemically bonded to inorganic sol–gel matrix materials.[25,27–35] Miura *et al.* reported that when an MPS–titania film with a 50 wt% MPS ratio was exposed for 10 seconds to 248 nm (deep UV or DUV) radiation having an intensity of 105 mW cm^{-2}, the refractive index of the film dropped by 0.18 while a MPS–silica film with a 50 wt% MPS ratio had a refractive index drop of 0.16.[29] These decreases in refractive indices were due to the incorporation of air within the matrix materials since air has a refractive index of only 1.0003 and thus will lower the aggregate refractive index of a material. While investigating the use of poly(methyl phenylsilane) (PMPS) films in the formation of phase masks, Nagayama *et al.* reported that 0.3 μm PMPS films exposed to 308 nm light had a refractive index drop from 1.70 to 1.63 while films exposed to 254 nm light showed a drop in refractive index from 1.70 to 1.58 due to photodecomposition of the PMPS.[25] Mimura *et al.* reported that when a MPS–silica (24 wt% MPS) hybrid film was exposed to UV radiation, the refractive index of the film dropped from 1.60 to 1.53 before rinsing with hexane, and dropped further to 1.40 after the hexane rinse leading them to conclude that all of the polysilane had decomposed.[28]

The polysilane-based photobleaching system described above relies on the direct photosensitivity of polysilane and will only work for polymers that can be directly decomposed by radiation. As opposed to polysilanes, polycarbonates, although not directly photocleavable, may be indirectly decomposed *via* UV radiation due to their vulnerability to acidolysis.[36,37] By mixing polycarbonate films with photoinitiators that release acids upon irradiation, *i.e.* photoacid generators (PAGs), the polymers molecules may be selectively decomposed *via* photogeneration of acids under a photomask thus enabling their use as positive-tone resist materials.[38–49] The mechanism for the acid-catalyzed depolymerization of both aromatic and aliphatic polycarbonates has been presented by Frechet *et al.* and Jayachandran *et al.*[36,37] The direct-write process presented here relies on the PAG–polycarbonate chemistry and it is an extension of the resist system in that both PAG and polycarbonate molecules are templated within a crosslinkable spin-on-glass (SOG) matrix. Prior to decomposition of the polycarbonate, the matrix is hardened to allow it to mechanically support porosity. UV exposure and a post-exposure bake (PEB) are used to drive acidolysis of the sacrificial polymer, resulting in the production of porosity and the lowering of the refractive index. By performing irradiation through a photomask, one may laterally pattern porous regions (cladding) and non-porous regions (cores) to create refractive index profiles within the processed film. To prevent acid-catalyzed decomposition of the polycarbonate molecules in non-porous regions, a blanket UV-irradiation is used to generate acids before their neutralization *via* the diffusion of a basic gas through the film. As an alternative to using a basic gas to neutralize the acid molecules, a vacuum environment or a high purge flow-rate may be used to sweep away volatile acid molecules after their photogeneration.

Experimental

The SOG matrix material was a resin of hydrogen silsesquioxane (HSQ) dissolved in methyl isobutyl ketone (MIBK) solvent and sold under the tradename FOx® by Dow Corning Corp. The sacrificial polymer used was poly(norbornene carbonate) or PNC which has the macromolecular structure **1**, shown in Fig. 1. Photobase generators (PBGs) refer to photoinitiators that release bases when activated by radiation.[46,47,50–56] The PBGs used in this study were n-cyclohexl-*p*-toluene sulfonamide (CTS), *o*-nitrobenzyl cyclohexylcarbamate (NBC), and *N*-methylnifedipine with their respective structures (**2**, **3**, and **4**) shown in Fig. 2. CTS and NBC were commercially obtained from Lancaster Synthesis and Midori Kagaku respectively. Since *N*-methylnifedipine was not commercially available, it was synthesized and purified according to the method reported in the literature and its structure, **4**, was verified by ^{1}H-NMR analysis.[57,58] The photoacid generators (PAG) used in this study were Rhodorsil 2074, tris(*tert*-butylphenyl)sulfonium triflate [TTBPS-Tf], and tris(*tert*-butylphenyl)sulfonium nonaflate [TTBPS-Nf], with their respective structures (**5**, **6**, and **7**) shown in Fig. 3. Rhodorsil 2074, TTBPS-Tf, and TTBPS-Nf were purchased from Rhodia, Sigma-Aldrich and Midori-Kagaku, respectively. HPLC grade MIBK solvent was obtained from Sigma-Aldrich and used without further purification.

Thermogravimetric analyses (TGAs) were used to obtain decomposition profiles of sacrificial polymer–PAG mixtures. For TGA studies, separate solutions of PNC and each PAG were made using MIBK solvent. These solutions were used to make PAG–PNC mixtures such that the solids content of dry PAG with respect to dry PNC was 3%. These mixtures were pipetted onto aluminium dishes and dried at about 110 °C for

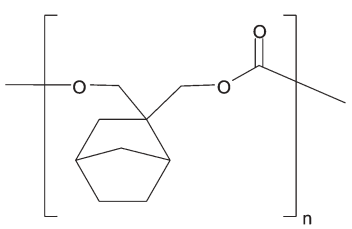

1

Fig. 1 Chemical structure of PNC repeating units.

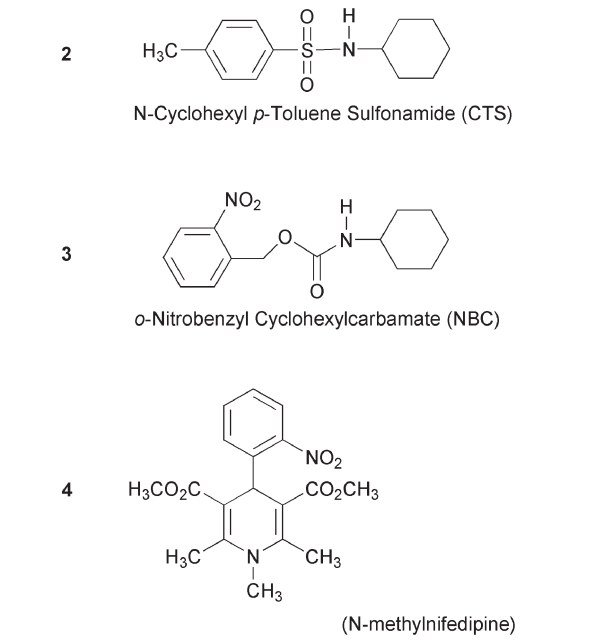

Fig. 2 Chemical structures of PBGs.

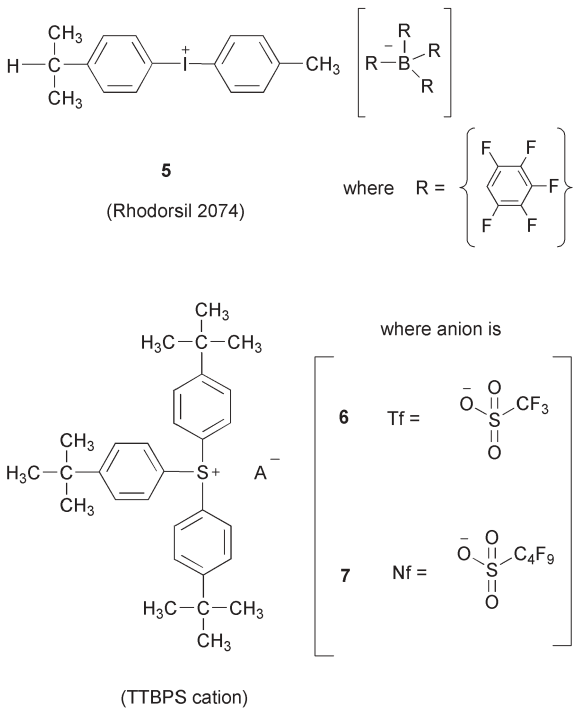

Fig. 3 Chemical structures of ionic PAGs.

1–2 hours in a vacuum oven prior to each TGA run in order to avoid the influence of solvent volatilization on the TGA results. Non-isothermal TGAs were performed by recording tared sample weights as the TGA oven was heated at 3 °C min^{-1} from ambient to about 325 °C and held at 325 °C for 90 minutes to completely decompose PNC. Isothermal TGAs were performed by recording tared sample weights only after ramping the TGA at 20 °C min^{-1} to the desired dwell temperature before tracking the weight of the sample against time. All TGA runs were performed with nitrogen purge flow-rates lower than 30 cm^3 min^{-1} to avoid the effect of acid volatilization on the rate of acid-catalyzed PNC decomposition. Differential scanning calorimetry (DSC) was used to determine the glass transition temperature of HSQ according to the method reported by Siew *et al.*[59] Both TGA and DSC studies were performed using a Sieko TG/DTA 320.

A Thermo-Nicolet 520 spectrophotometer was used to perform FTIR studies on spin-coated HSQ films of 0.7–1.2 μm thickness using attenuated total reflectance (ATR) mode. A Hysitron Triboindenter was used to perform nanoindentation studies on the HSQ films after FTIR analysis. During nanoindentation, the films were probed multiple times using a Berkovich tip according to the method outlined by Oliver and Pharr.[60–62]

For porous films formed *via* the traditional template technique, a dilute solution of PNC in MIBK solvent was mixed with Fox-1x® resin to make mixtures with the mass ratios of PNC to dry HSQ ranging from 1 : 10 to 3 : 10. These solutions were spin-coated onto silicon wafers and then the films were heated in a nitrogen-purged Lindberg furnace at 3 °C min^{-1} from 270 °C to 325 °C and held at 325 °C for 90 minutes to completely decompose PNC. The properties of these thermally processed porous films were compared to those of pure HSQ control films that underwent the same heating procedure to elucidate the effect of induced porosity on the average properties of the matrix.

For direct-write processing of thin films, separate dilute solutions were made for the following substances in MIBK solvent: CTS, *N*-methylnifedipine, TTBPS-Tf, and PNC. Fox-1x® resin was used as supplied from Dow Corning. Although both CTS and *N*-methylnifedipine PBGs were thermally unstable, their absorbance spectra were very different (CTS was highly absorptive at wavelengths <300 nm and *N*-methylnifedipine was highly absorptive up to 400 nm). Owing to the different properties of the PBGs, two separate types of direct-write formulations were made, named A and B.

For A-type formulations, the separate solutions of CTS, TTBPS-Tf, PNC, and Fox-1x® resin were mixed to produce the following mass ratios with respect to dry solids: wt PBG to wt PAG to wt PNC to wt HSQ = 1 : 2 : 2 : 20. For B-type formulations, the separate solutions of *N*-methylnifedipine, TTBPS-Tf, PNC, and Fox-1x® resin were mixed to produce the following mass ratios with respect to dry solids: wt PBG to wt PAG to wt PNC to wt HSQ = 1 : 5 : 10 : 50 and 1 : 10 : 20 : 100. Both types of direct-write solutions were passed through 0.2 μm PTFE membrane filters prior to spin-coating onto silicon wafers to avoid film non-uniformities arising from the presence of particulates.

The basic sequence for the direct-write process reported in this paper is shown in Fig. 4. The first step involved the dispensing of a solution containing an SOG material, a sacrificial polymer (porogen), and a photoacid generator (PAG) onto silicon wafer. The spin-coated film was then cured or hardened below the thermal activation temperature of the PAG to avoid decomposing the sacrificial polymer throughout the film. The low-temperature curing occurred *via* base-catalyzed gelation of the SOG matrix where the bases used were either ammonia gas or photogenerated bases released from activated photobase generator (PBG) species

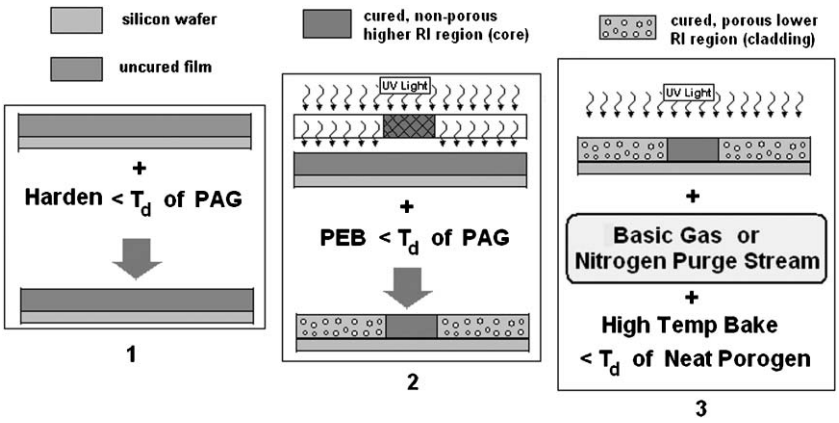

Fig. 4 Basic sequence for lateral patterning of direct-write porosity. T_d refers to the temperature at which degradation begins.

incorporated in the formulation of the dispensed solution. To crosslink A-type spun films, the samples were placed in a Lindberg furnace already at 160–170 °C and baked for 30 minutes in stagnant air. The baking activated the CTS PBG molecules resulting in the release of cyclohexylamine, which catalyzed the gelation of HSQ.[52,56] Since *N*-methylnifedipine could be activated either thermally or by UV exposure >300 nm, B-type spun films were crosslinked either by a similar bake procedure to A-type films or exposed to 1 J cm^{-2} of 365 nm UV underneath a filter to prevent DUV from reaching the samples and prematurely activating the TTBPS-Tf PAG followed by a post-exposure bake (PEB) above 120 °C in a Lindberg furnace in stagnant air. After the crosslinking step shown in Fig. 4, the direct-write films were exposed to DUV radiation under a light field quartz photomask with a PEB to activate the PAG and release acid in irradiated regions and hence selectively decompose the sacrificial polymer. To prevent PNC decomposition in unexposed regions and thus maintain the refractive index profile, films were blanket exposed with DUV radiation to activate remaining PAG, followed by either volatilization of acid molecules at high temperature or immediate treatment with a basic gas (ammonia gas) to neutralize the photogenerated acids at ambient temperature. Finally, the films were heated to about 250 °C for 30 minutes while purging the tube furnace with 2 L min^{-1} flow-rate of nitrogen in order to drive off any polar species and condense residual silanol groups within the SOG matrix, since both would degrade the film's low-*k* and optical properties by encouraging moisture uptake. Direct-write control films (HSQPBGPAG), which had the same HSQ, PBG, and PAG loadings as direct-write formulations without any PNC content, were processed in a similar manner to direct-written films to determine the effect of porosity on the average properties of the direct-written matrix. UV-patterned films were processed in a similar manner except a quartz photomask containing opaque line patterns was used during the DUV exposure to define features on the film.

A Oriel 92521 floodlit lamp was used to carry out blanket DUV exposures whereas a Karl-Suss MJB-3 contact aligner and photomask were used for direct-writing of lateral porosity patterns. DUV intensities were measured at 240–250 nm using calibrated UV intensity probes. A J. A. Woollam M2000 VI spectroscopic ellipsometer (VASE) was used together with a Cauchy model to find the refractive index values of porous and non-porous films during processing. All refractive indices reported are for a wavelength of 632 nm and, when necessary, the extinction coefficients of the processed thin films were also fit using the ellipsometer's WVASE software. To track the refractive index differences between core and cladding areas in A-type and B-type samples during processing, one half of each sample was covered with a polished wafer while the other half was exposed to at least 3.8 J cm^{-2} of DUV radiation to activate the PAG, followed by a PEB for at least 20 minutes in a Lindberg furnace at 160–170 °C in stagnant air during which the PNC in the exposed regions was decomposed by triflic acid. Finally the remaining PAG molecules were activated and the generated acid was neutralized using ammonia gas and then polar species were removed by baking the films in a Lindberg furnace at 250 °C while using a nitrogen purge stream to sweep away volatilizing substances.

In order to determine the interline dielectric constant of porous and control films, interdigitated electrodes (IDEs) were fabricated on oxidized silicon wafers, each with 200 comb-like fingers connected to each bond pad, such as the one shown in Fig. 5. Using the lift-off technique (photolithography followed by metal deposition onto patterned photoresist, followed by photoresist removal), IDEs were patterned with 5 μm wide

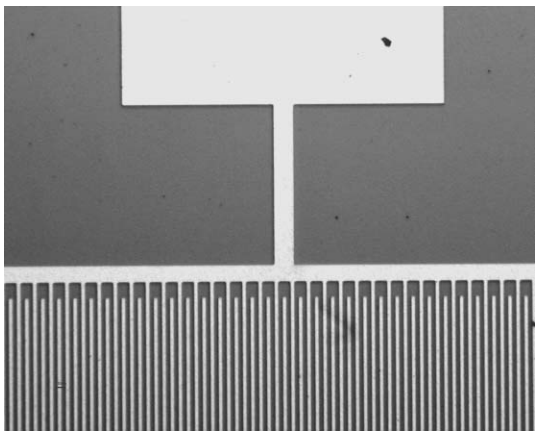

Fig. 5 Microscope image showing the top-down view of an IDE.

metal lines and 5 μm wide gap spacing between each metal line. An e-beam evaporator was used to deposit 10–15 nm of titanium followed by 200 nm of gold at high vacuum onto at least 10 μm thick plasma-enhanced chemical vapor deposition (PECVD) silicon dioxide. A Tencor KLA profilometer and calibrated microscope were used to measure the actual dimensions of the IDEs and a Nanospec refractometer was used to measure the thickness of the PECVD oxide layer. An HP 4253 LCR meter and Karl Suss PM5 probe system were used to measure the capacitances of multiple IDEs at a frequency of 100 kHz both before and after spin-coating the silicon wafers with films. After spin-coating films onto the IDEs, portions of the films were scraped to allow thickness measurements after each processing step using the profilometer. The thicknesses of the coated films ranged from 280 nm to 430 nm and the capacitances of the coated IDEs were remeasured after each processing step. Using the measured dimensions of the IDEs, and the measured thicknesses of the oxide and coated films, electrostatic simulations (Ansoft's Maxwell software) were used to accurately model the capacitances of the IDEs and thus empirically determine the interline dielectric constant of the films.

Atomic force microscope (AFM) scans were performed using a Veeco Dimension 3100 scanning probe microscope. In order to characterize the pore structure of porous films, focused gallium ion beams (FIB) were used to prepare thin cross-sections of samples after first sputtering these films with protective gold and platinum layers to prevent gallium implantation during milling. These thin cross-sections were then analyzed using a Hitachi HF-2000 high resolution TEM operated using an accelerating voltage of 200 keV.

Results and discussion

The selective decomposition of sacrificial polymer in the direct-write process depicted in Fig. 4 relied on the ability of the sacrificial polymer to be selectively decomposed by photogenerated acids, *i.e.* it was photodefinable. The mechanism by which photogenerated acids catalyzed the decomposition of polycarbonate-based sacrificial polymers has been discussed in the literature.[36,37] According to the reported mechanism, protons from the acid attack the carbonyl group of a polycarbonate, such as the one shown in Fig. 1, resulting in main chain scission of the sacrificial polymer and the evolution of volatile decomposition products. Researchers have used TGA studies of sacrificial polymer–PAG mixtures to study the acid-catalyzed decomposition of polycarbonate-based polymers.[36,37] The larger the temperature difference between the onset of the photolytic decomposition (irradiated PAG) TGA curve and the thermolytic decomposition (PAG heated only) TGA curve for a polymer–PAG mixture, the wider the temperature window for the PEB, *i.e.* the higher the likelihood of decomposing most or even all of the polymer in the exposed region without decomposing any of the PNC in the unexposed region of the wafer. Thus PAG–PNC mixtures with the largest differences between thermolytic and photolytic TGA curves were deemed optimal for use in the PAG–polycarbonate direct-write formulations since they could be used for producing both blanket as well as patterned porosity within films.

Numerous PAGs that produce strong acids were tested for their thermal stability, possessing the chemical structures shown in Fig. 3.[37] In order for a PAG to be compatible with selective decomposition of the photodefinable polymer, it must have a high thermal stability. Otherwise, direct-written refractive index profiles in a film will be destroyed upon heating the film to moderate temperatures due to the thermal activation of the PAG. PAGs with diphenyl iodonium cations tend to have low thermal stability as can be seen in the TGA plot of Rhodorsil 2074–PNC mixtures shown in Fig. 6.[37,47] The temperature at which Rhodorsil 2074 spontaneously decomposes to produce an acid (thermal acid generation) is not significantly higher than the PEB temperature required to form acid after UV exposure indicating that the acid [hydrogen tetrakis(perfluorophenyl)borate or HTPFPB] would be likely to be released throughout a direct-write film containing this PAG. Therefore, sacrificial polymer chains in both exposed and unexposed regions would be decomposed by the acid molecules and so selective decomposition would not be achieved if PAGs with such a low thermal stability were used.

Ionic PAGs with cations derived from the photosensitive triphenyl sulfonium moiety are attractive due to their high thermal stability relative to diphenyl iodonium PAGs.[47] As seen in Fig. 7, TTBPS-Tf has the following desirable properties: relatively high thermal stability with respect to the PEB temperatures required to decompose PNC after UV exposure as well as the ability to decompose PNC rapidly due to the high strength of the photogenerated acid (triflic acid).[47] Further TGA studies showed that TTBPS-Nf had desirable properties similar to TTBPS-Tf as seen in Fig. 8. Hence it was determined that TTBPS-Tf and TTBPS-Nf were suitable PAGs to incorporate in the direct-write system.

In order for the SOG matrix to mechanically support porosity, it must be rigid enough to avoid pore collapse during decomposition of the sacrificial polymer. In conventional SOG processing, the resins are spin-coated onto silicon wafers to form planar dielectric films that become rigid when heated above their glass transition temperature.[61,63,64] Although HSQ is typically thermally cured above 350 °C, researchers reported

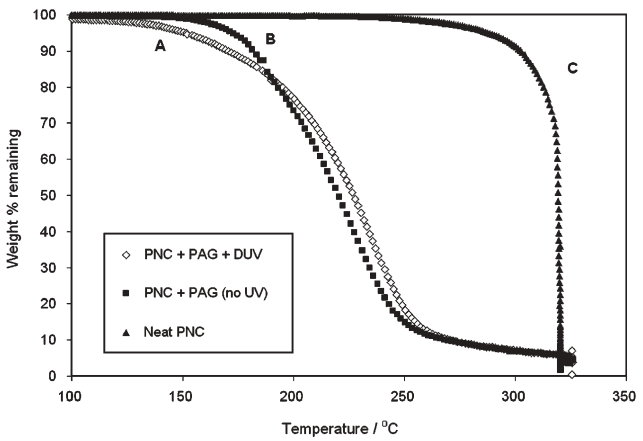

Fig. 6 Non-isothermal TGAs of (A) a PNC–Rhodorsil 2074 mixture exposed to 1 J cm^{-2} DUV radiation, (B) an unexposed PNC–Rhodorsil 2074 mixture, and (C) pure PNC ramped at 3 °C min^{-1} to 325 °C.

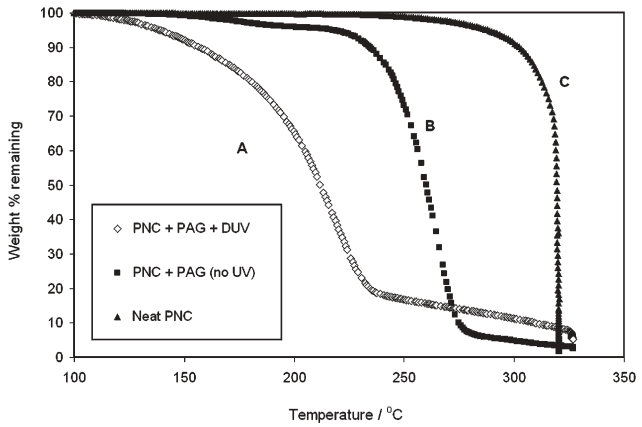

Fig. 7 Non-isothermal TGAs of (A) a PNC–TTBPS-Tf mixture exposed to 1 J cm^{-2} DUV radiation, (B) an unexposed PNC–TTBPS-Tf mixture, and (C) pure PNC ramped at 3 °C min^{-1} to 325 °C.

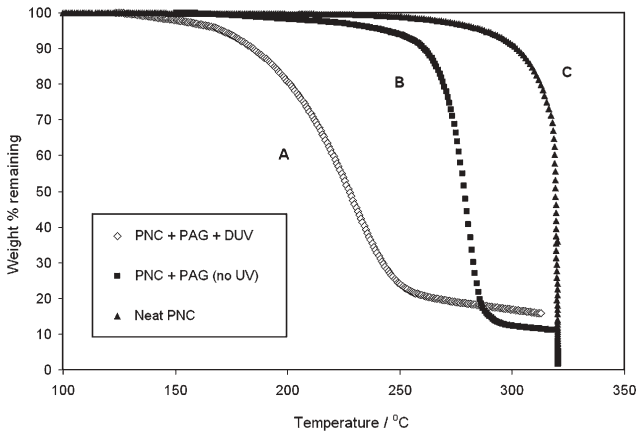

Fig. 8 Non-isothermal TGAs of (A) a PNC–TTBPS-Nf mixture exposed to 1 J cm^{-2} DUV radiation, (B) an unexposed PNC–TTBPS-Nf mixture, and (C) pure PNC ramped at 3 °C min^{-1} to 325 °C.

evidence for HSQ cure reactions below 350 °C and we have successfully hardened HSQ by baking them at 200 °C for 2 hours.[61,63,64] To determine the compatibility of thermal curing with the direct-write process shown in Fig. 4, isothermal TGA studies of TTBPS-Tf–PNC mixtures were performed for several temperatures above and below the glass transition temperature of the HSQ matrix (194–195 °C determined by DSC).[59] The results of the isothermal TGA experiments, shown in Fig. 9, indicated that above the glass transition temperature, the PNC–PAG mixtures experienced significant weight loss and the rate of weight loss increased with increasing temperature. This is because at temperatures above 195 °C, TTBPS-Tf was thermally activated to produce triflic acid, leading to acid-catalyzed decomposition and volatilization of PNC. However, at temperatures below 195 °C, the PNC–PAG mixture experienced a total weight loss of less than 5 wt% even after being heated isothermally for up to 2 hours, thus showing that the PAG was thermally stable at temperatures below the glass transition temperature of the HSQ matrix. Ellipsometry provided further evidence for the thermal activation of PAGs above the glass transition temperature of HSQ in that the refractive index of HSQ–TTBPS-Tf–PNC

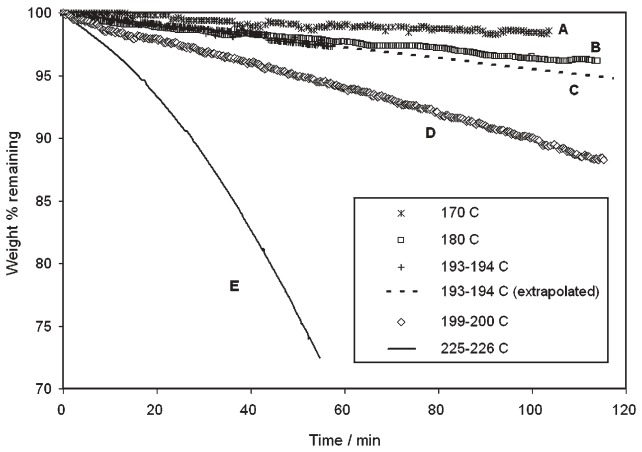

Fig. 9 Isothermal TGAs of unexposed PNC–TTBPS-Tf mixtures held at (A) 170 °C, (B) 180 °C, (C) 193–194 °C [with experimental data extrapolated past 60 min], (D) 199–200 °C, and (E) 225–226 °C.

films with a PNC loading of 10% dropped from 1.413 to 1.365 when heated at 200 °C for 2 hours without any prior irradiation whereas that of non-porous control films (no PNC) remained at about 1.38 after undergoing the same bake conditions.[64] Hence the curing of HSQ above its glass transition temperature was deemed incompatible with the direct-write process because it would lead to the thermal activation of the PAG and hence the decomposition of PNC throughout the film. However, due to low chain mobility, the thermal curing of HSQ below its glass transition temperature occurs on too large a timescale for feasible mass fabrication of direct-write films.

To harden HSQ relatively quickly while simultaneously avoiding thermal activation of the PAG in the direct-write process, bases were used to catalyze the hydrolysis of the silane bonds in HSQ to form silanol groups at relatively low temperatures.[65–67] These silanol groups were highly reactive and condensed to form siloxane bonds thus increasing the rigidity of the film.[9,11,57,58,68,69] This low-temperature gelation reaction was used during the first of the processing steps shown in Fig. 4 to make the HSQ matrix rigid enough to support porosity without the problems associated with thermal activation of the PAG. A possible mechanism for the hydrolysis of silanes, proposed by Sommer, involves the induced polarization of the silicon center by a nucleophile followed by the attack of the electropositive silicon center by a water molecule as shown in Scheme 1.[66] The d-orbitals present in silicon atoms allow silicon centers to form pentacoordinate

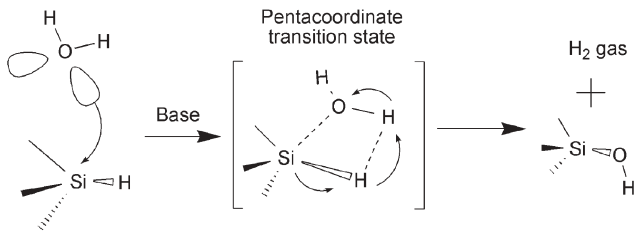

Scheme 1 The S_ni-Si mechanism of silane hydrolysis proposed by Sommer.[66]

and hexacoordinate transition states during reactions.[65] There is an internal rearrangement of the temporary bonds in the transition state that leads to a silanol group replacing the silane group as shown in Scheme 1.[66] According to West, the hydrolysis of cyclic silanes such as HSQ cages is thermodynamically favorable because the pentacoordinate transition state relieves the bond strains present in the original cyclic structures.[67]

According to the literature, the FTIR spectrum of HSQ has stretch peaks centered at 2250 cm^{-1}, 1130 $cm^{-1}$and 1070 cm^{-1} corresponding to silane, cage-type siloxane, and network-type siloxane bonds respectively.[62–64,69] When spin-coated HSQ films were exposed to ammonia gas, the FTIR stretch peak due to the silane bonds decreased and a small peak centered at 3740 cm^{-1} appeared, as shown in Fig. 10a. The new peak arose from the formation of silanol bonds hence supporting Sommer's hypothesis that silane bonds are converted to silanol bonds during gelation.[66] Silanol bonds are very reactive and subsequent condensation of adjacent silanol bonds resulted in the formation of network-type siloxane bonds thus increasing the area of the siloxane network peak in the FTIR spectra.[9,11,57,58,68,69] The ammonia treatment also caused the siloxane cage-type peak to decrease and the peak corresponding to siloxane network-type bonds to increase, as shown in Fig. 10b. The decrease in cage-type siloxane peaks was due to the scission of these bonds *via* base-catalyzed hydrolysis, which resulted in the opening up of the cage structure to form a pentacoordinate transition state.[67] The transition state then preferentially rearranged during condensation to form an open network structure, which had less bond strain than the closed cage structures as described by West.[67] Hence, during gelation, the ratio of siloxane cage to siloxane network peak areas decreased, and as done by other researchers, this ratio was used as a measure of the extent of HSQ crosslinking reaction.[64,69] Similar to methods cited in the literature, photobase generators (PBGs) were mixed in formulations in order to harden the matrix upon activation of the PBG *via* blanket UV exposure or by thermal activation.[52,53,56–58,70,71] Once activated, the PBGs released bases that catalyzed the cross-linking of HSQ units *via* the sol–gel condensation of silanol bonds formed from the hydrolysis of silane bonds and rearrangement of hydrolyzed cage-type siloxane bonds to network-type bonds.[57,58] The average reduced moduli (E_r) of films gelled using either a basic vapor (ammonia gas) or a photogenerated base are shown in Fig. 11 along with their respective FTIR cage/network peak area ratios.

It can be seen from Fig. 11 that the reduced modulus of gelled films increased as the cage/network peak area ratio decreased.[61,62,69] This confirmed that as the relative amount of networked siloxane bonds to cage bonds increased, the HSQ matrix became more rigid. HSQ films that were exposed to saturated ammonia vapor for 3 minutes at ambient conditions had a final E_r of 3.65 GPa. This was observed to be about the same rigidity of gelled HSQ–PBG films with initial CTS or NBC loadings of about 3 wt% with respect to dry HSQ. The loading of *N*-methylnifedipine required to give an equivalent reduced modulus after activation of the PBG was only 1 wt% with respect to HSQ. As shown in Fig. 12, when compared on the basis of equivalent loading weight in HSQ, the *N*-methylnifedipine PBG is the most efficient at crosslinking HSQ. Since the molecular weight of *N*-methylnifedipine is the largest of the three PBGs studied, then even on a molar basis the alkylammonium hydroxide base it releases is much more efficient at hardening HSQ than the cyclohexylamine base

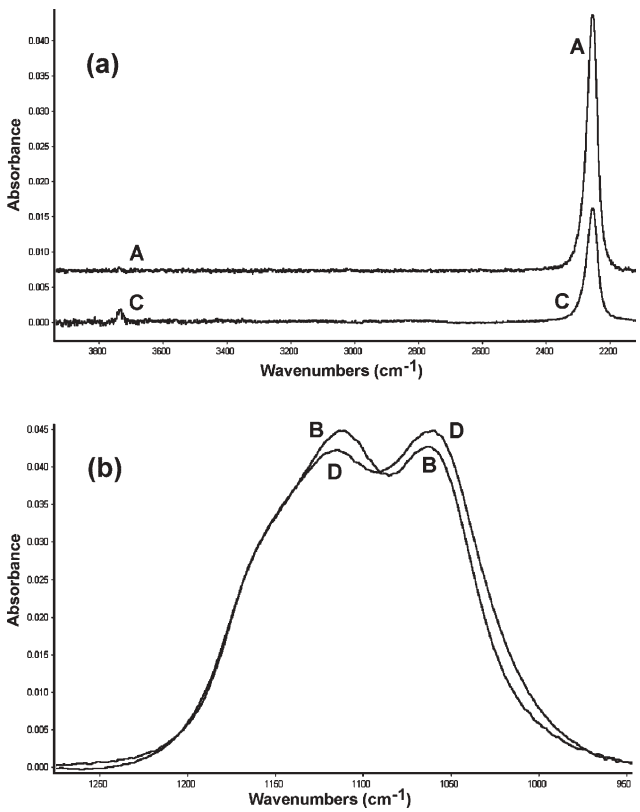

Fig. 10 (a) Comparison of the silane and silanol content of HSQ films gelled for (A) 0 min and (C) 5 min using ammonia gas at 25 °C. The baseline of curve A was offset for clarity. (b) Comparison of cage and network-type siloxane peak in HSQ films gelled for (B) 4 min, (D) 10 min using ammonia gas at 25 °C.

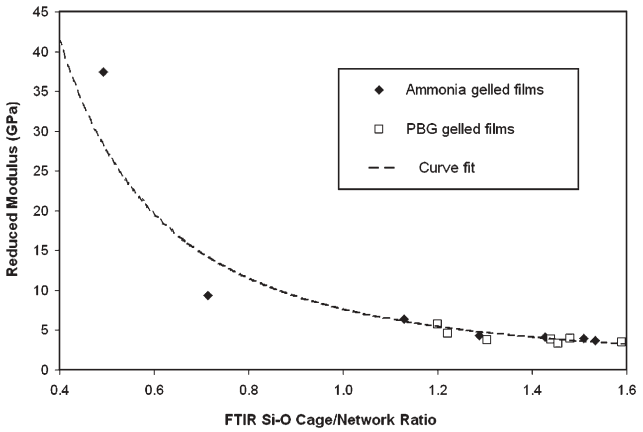

Fig. 11 Plot showing correlation between reduced modulus and FTIR spectra siloxane cage/network stretch peak area ratios for HSQ gelled using (◆) ammonia vapor and (□) UV-released bases from PBGs. For clarity, a curve fit (– – –) is used to show the trend in the data.

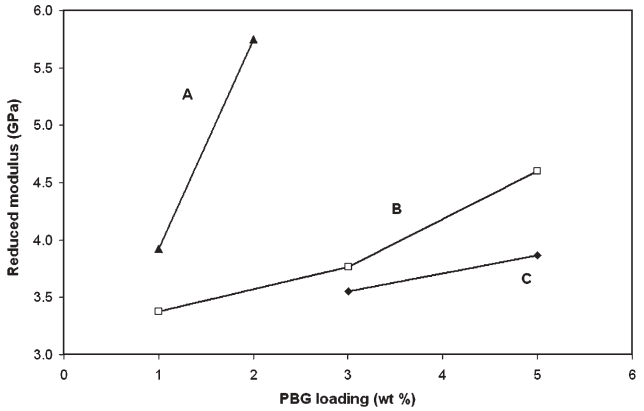

Fig. 12 Relative comparison of mechanical rigidity induced by bases released by (A) *N*-methylnifedipine, (B) NBC, and (C) CTS at different PBG loading levels.

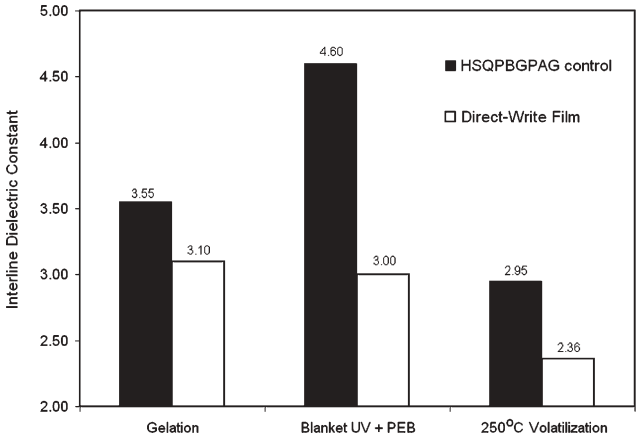

Fig. 13 Comparison between the interline dielectric constants values (at 100 kHz) of blanket irradiated direct-written and control films during processing. Their PNC loadings were 20 wt% and 0 wt%, respectively.

released by the other two PBGs.[53,56–58,70,71] The presence of direct-written porosity in cladding areas was indicated by refractive index values dropping below that of pure HSQ control films (1.389) that underwent similar heating cycles. By using the Lorentz–Lorenz refractive index mixing rule to estimate induced porosity, it was observed that the level of rigidity needed for direct-written films to be able to support 10 vol% porosity corresponded to E_r values of at least 3.5 GPa while 20 vol% porosity required E_r values of over 4 GPa. Films with E_r less than 3.1 GPa after gelation had refractive indices equal to that of the HSQ control samples after decomposition of PNC, which implied that in these films the matrix was not rigid enough to support porosity because pores that were formed ultimately collapsed resulting in non-porous HSQ films.

During the deactivation step shown in Fig. 4, no drop in refractive index was observed in core regions even though the bake temperature (250 °C) exceeded the thermal activation point of the TTBPS-Tf PAG (see Fig. 9). This indicated that all the photogenerated acid had been either neutralized or volatilized; hence, there was no acid-catalyzed decomposition of polycarbonate. The thermal stability of the refractive index profile was only limited by the onset of decomposition of the neat PNC polymer, which according to the TGAs of neat PNC was about 270 °C (see Fig. 5–7). Hence for high thermal stability of UV-defined patterns of porosity, it was desirable to use a photodefinable porogen with as high a decomposition point as possible in the direct-write system.

Fig. 13 compares the interline dielectric constants of the direct-written films (with 20 wt% PNC loading) to their control samples for each step of the direct-write process shown in Fig. 4. After gelation, the matrix had a relatively high dielectric constant compared to pure HSQ (k = 2.80) due to the effect of the PBG-released bases on the average polarizability of the films. After gelation, the direct-write film had a slightly lower dielectric constant than the control sample due to the effect of the free volume occupied by the polymer on the polarizability of the direct-write matrix. After UV exposure, the dielectric constant of the control sample rose dramatically owing to the large increase in polarizability that was caused by the photogeneration of acids. The dielectric constant of the direct-write film dropped slightly after UV exposure because the porosity induced in the matrix backbone mitigated the effect of the increased polarizability from acids. The high temperature volatilization of the acids caused a decrease in the dielectric constants of both the porous and control films since the removal of polar species lowered the polarizability. The final dielectric constant of the control sample was slightly higher than that of HSQ (k = 2.80), probably as a result of increased film density due to catalyzed crosslinking in the previous steps. The direct-written film exhibited a much lower dielectric constant than the control due to the induced porosity within the matrix. Porous films formed *via* the traditional template technique and at the same polymer loading as the direct-written film had interline dielectric values of 2.29 compared to a value of 2.80 for its control film. Using the Maxwell–Garnett mixing rule to compare the final the interline dielectric constants of the porous and non-porous films, the level of UV-induced porosity was estimated to be 21 vol% for the direct-written films and 20 vol% for the thermally-processed films.

Although porosity is formed when irradiated films were heated at 170 °C, the volatilization step, which is performed at 250 °C, is necessary in order to achieve a low-k value. This indicates that the direct-write process presented here is limited to substrates capable of withstanding baking temperatures of 250 °C. The use of PBGs and PAGs in the direct-write process also had an undesirable effect on the overall polarizability of the HSQ matrix since the interline dielectric constant for direct-written porous films (k = 2.36) was slightly higher than that of thermally-processed films (k = 2.29) even though the UV-induced porosity was slightly higher than the thermally-induced porosity. This is because the non-porous backbone of direct-written films (k = 2.95) have a higher dielectric constant than pure HSQ (k = 2.80). This may be a result of the presence of by-products of the PAG photocleavage reactions remaining in the film after volatilization of the acid. Based on the chemical structures reported in the literature, the by-products of PAG activation have permanent dipoles; hence, these species would increase the polarization of the matrix and cause

the dielectric constant to be higher than that of a pure HSQ film.[48,49]

Two scenarios would allow the final polarizability of direct-written films to be lowered even further. If an alternative matrix material could be crosslinked at low temperatures without the need for base catalysis, then the required PAG content would be much lower since no bases would be present to partially neutralize the acid molecules. The mass ratio of PAG to polymer used in the TGA studies was only 3 wt%, thus the absence of PBGs in such a direct-write system would allow PAG loadings to be lowered by at least one order of magnitude. If the acid content was sufficiently low, the volatilization step may become unnecessary, hence allowing more substrates to be used for direct-write processing of low-*k* films. An alternative case would involve the use of a base that was more efficient at crosslinking HSQ than the base released by *N*-methylnifedipine. The greater mechanical integrity would allow higher levels of UV-induced porosity to be incorporated within the direct-written matrix hence allowing lower values of the dielectric constant of the direct-written films after the volatilization step.

Fig. 14 shows values of refractive index of the exposed and unexposed halves of an A-type film having PBG, PAG and PNC loadings of 5%, 10%, and 10%, respectively. The refractive index on the irradiated side dropped to 1.344 due to the incorporation of porosity within the matrix while the refractive index of an A-type HSQPBGPAG control that underwent the same treatment was 1.379. The refractive index values were observed to be very low even directly after the UV exposure and PEB step because optical frequencies ($\sim 10^{14}$ Hz) are above the maximum frequencies for orientation and distortion polarization. Thus residual acid and base had a much lower influence on refractive index measurements than on dielectric constant measurements.[1] As further evidence of this, the refractive index values of HSQPBGPAG controls were found to be similar to those of pure HSQ films after both the second and third steps of the direct-write process. Using the Lorentz–Lorenz refractive index mixing rule, we estimated that air occupied about 8% of the volume in the irradiated side.[1,16,17,22] The refractive index in the unexposed half of the wafer was fairly constant during the PEB because the unexposed PAG was thermally stable during the 170 °C bake, hence there was the absence of acidolytic decomposition of the PNC. The slight rise in refractive index of the unexposed side of the A-type film during the deactivation step shown in Fig. 14 was probably due to an increase in density from film shrinkage caused by the condensation of dangling silanol bonds during the 250 °C bake.

Due to the high efficiency of *N*-methylnifedipine PBG at crosslinking HSQ once activated, we were able to mechanically support higher levels of porosity in B-type films than we could use in A-type films prior to seeing the effects of pore collapse. For B-type films with PBG, PAG and PNC loadings of 2%, 10%, and 20%, respectively the final refractive index on the irradiated side was 1.313 compared to a value of 1.398 for a B-type HSQPBGPAG control film.[1,16,17,22] Hence, for B-type films, the difference in refractive index between the porous region and a HSQPBGPAG control sample was as high as 0.085, which by using the Lorentz–Lorenz equation indicates that the amount of porosity incorporated on the irradiated side was about 20 vol%. Thermally processed porous films with the same loading (20 wt%) had refractive index values of 1.302 compared to a value of 1.394 for a pure HSQ control that underwent the same heating procedure. The amount of thermally-induced porosity was estimated to be 21 vol% using the Lorentz–Lorenz equation. The final values of the refractive index of UV-induced porous films appear reasonable in that they are similar to those of thermally-processed porous films of the same polymer loading and also similar to other templated films reported in the literature.[7] The decreases in refractive index values of the PAG–polycarbonate direct-write system are also comparable to the photobleaching direct-write system reported in the literature and the differences may be attributed to the differences in loading levels of the decomposable polymers used.[25,28,29]

The levels of porosity estimated using refractive index mixing rules were quite close to those predicted by dielectric constant mixing rules and differences are likely to be a result of uncertainties in film thickness arising from the rough surfaces of the porous films, such as the film shown in Fig. 15.[6,33,72]

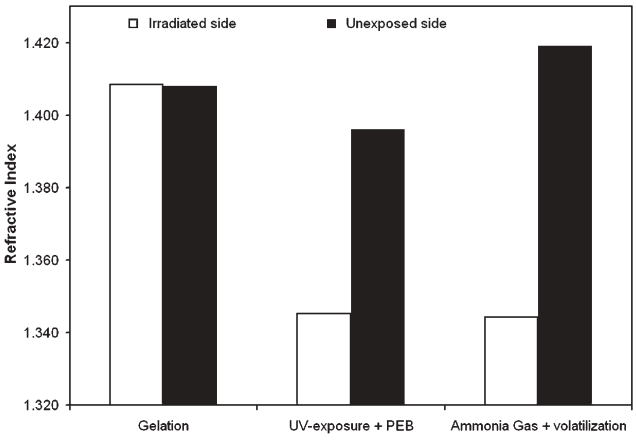

Fig. 14 Refractive index values on irradiated and unexposed halves of an A-type direct-write film after sequential processing steps. The PNC loading was 10 wt%.

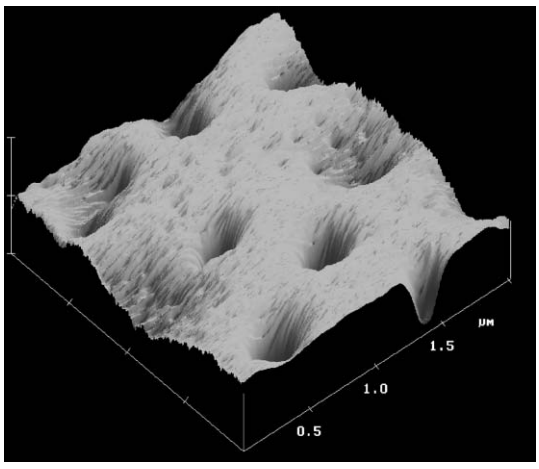

Fig. 15 AFM image of the irradiated side of a direct-write film having a PNC loading of 20%. The rms roughness values of the unexposed and irradiated sides were 7.3 and 14.5 nm, respectively.

The surface roughness of porous films scaled with the initial PNC loading, for both UV-exposed and thermally-processed films. For direct-written films with 20% PNC loadings, the unexposed and UV-irradiated sides had rms surface roughness values of 7 nm and 14 nm respectively, while thermally-processed films of the same PNC loading had an rms surface roughness values of 26 nm. The sizes of pits on the surface of both direct-write and thermally-processed porous films varied widely with their depths ranging from 60–150 nm and their lateral dimensions were of the order of hundreds of nanometers for direct-written films and from hundreds of nanometers to 1.5 μm for thermally-processed films. Although the degree of surface roughness increased with increasing polymer loading, there did not seem to be any correlation between the polymer loading and the dimensions of the pits. Light scattering induced by the surface roughness gave the porous films a hazy appearance and would have adversely affected the optical characterization of the films hence increasing the uncertainty of the refractive index values and any porosity estimated using them. The roughness would have had a lower influence on the electrical characterization because the average film thicknesses (280–430 nm) were much larger than the values of rms roughness of the films and the uncertainty induced in modeling the IDEs would be small. For this reason, the porosity estimates based on the dielectric constant data are more reliable than that calculated using optical data.

Fig. 16 and 17 show TEM images of the microstructure of a thermally-induced porous film and a UV-induced porous film, respectively. Both films had a polymer loading of 20% and, based on porosity estimates from dielectric constant mixing rules, their induced porosities were very similar (21% and 20%, respectively). It is clear by comparing the structures shown in Fig. 16 and 17 that there are significant differences in the internal structures of these films. From Fig. 16, we observe that using the traditional template technique (thermally-induced decomposition of PNC) produced closed-cell mesopores (5–10 nm in size) that were nearly spherical in shape and located in close proximity to one another (the bright, elongated 'spongy' areas are collections of mesopores). The agglomeration of the mesopores in large patches was likely due to phase segregation and agglomeration of polymer chains prior to decomposition, which was encouraged by the high processing temperatures of the template method. As the PNC thermally decomposed, the mesopores formed in relatively close proximity to one another and the pores may have preferentially collected as a result of internal forces acting on them. The lack of bonding groups on the backbone of PNC, **1**, negated the possibility of avoiding phase segregation *via* the chemical bonding of the polymer to HSQ prior to heating.[2–4,6] Although the mesopores shown in Fig. 16 were in large collections, no macropores were detected and thus complete agglomeration of polymer chains prior to decomposition did not occur.

From Fig. 17, we observe that direct-written films contain two different sizes of UV-induced pores within the film: elongated mesopores (measuring 10 nm by about 20–30 nm), and elongated macropores (measuring 100 nm by about 200 nm). The intrinsic structure of HSQ contains micropores (measuring 1–2 nm), which are visible in the lower right corner of Fig. 17, where they are situated behind a macropore bubble that was conveniently sliced during FIB milling. Thus the micropores are not a result of PNC decomposition and are naturally present in every SOG film regardless of the type of processing it underwent. The isolated mesopores shown in

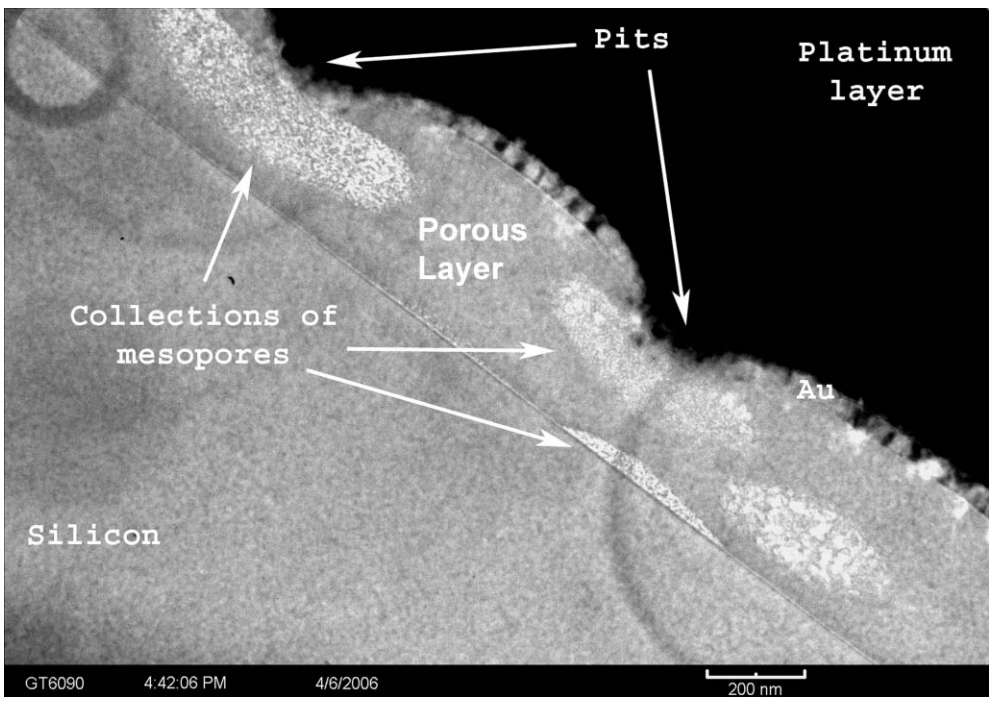

Fig. 16 TEM image of a thermally-processed film with a 20% PNC loading after thermal decomposition of the polymer at 325 °C. Image taken at a magnification of 30 000.

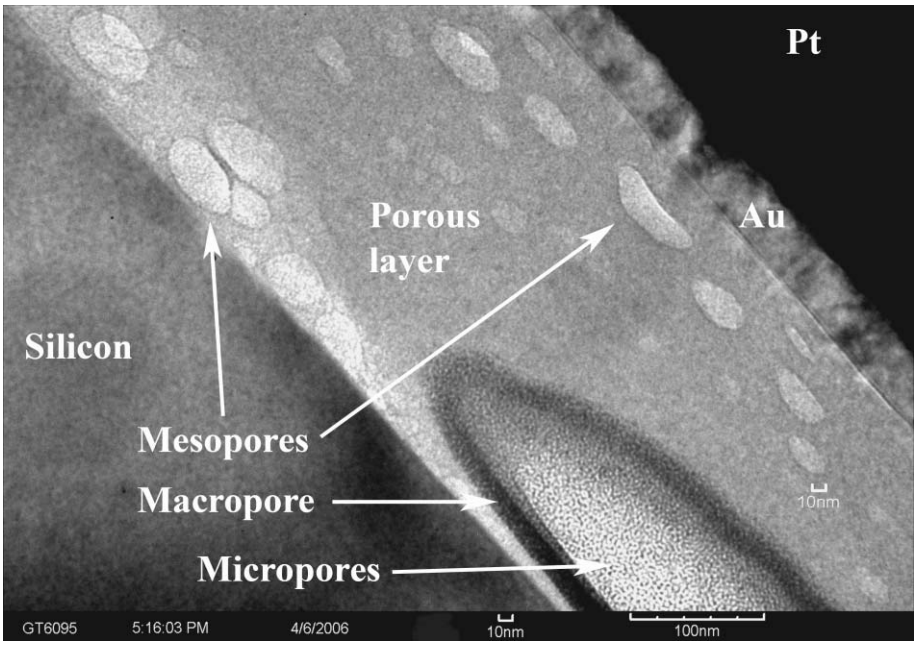

Fig. 17 TEM image of a B-type direct-write film with a 20% PNC loading after the UV-decomposition of the polymer without a 250 °C volatilization step. Image taken at a magnification of 100 000.

Fig. 17 were induced by the decomposition of PNC and they were not present in large collections such as the ones shown in Fig. 16, suggesting that the lower temperature processing of direct-write films does not encourage large scale movement of polymer chains prior to decomposition. The macropore shown in Fig. 17 is likely due to the coalescence of meso-sized air pockets after decomposition possibly as a result of rapid film shrinkage induced by acid-catalyzed condensation of residual silanol bonds generated during the gelation step. Film shrinkage would also account for the shape of the meso-sized and macro-sized pores, which all appear to be thinner in the vertical direction and wider in the lateral direction. The thermally-processed film, shown in Fig. 16, did not contain any crosslinking agents but gradual film shrinkage may have occurred during polymer decomposition thus leading to the elongated groupings of mesopores. The TEM images of thin A-type direct-write films showed pores of similar shapes and sizes to the B-type direct-write film shown in Fig. 17 but the amount of pores in A-type films was fewer since these films were less crosslinked and could not support more than 10% of UV-induced porosity.

The pits shown in Fig. 16 were only present when collections of pores were in close proximity to the surface. This indicated that the evolution of a relatively large volume of gaseous decomposition products near the surface was the likely cause of disruptions on the film surface that led to the formation of depressions. By comparing lateral dimension of the spongy patches and the pits in Fig. 16, it is clear that the sizes of the pits are largely dependent on the underlying internal structure. It was also observed that when the macropores of UV-exposed direct-write films were situated close to the surface of the films in the TEM images, pits appeared directly above them on film surface, with similar characteristics to those of thermally processed films. However, as seen in Fig. 17, when macro-sized pores are not adjacent to the film surface, no pits are present above them. Additionally, the isolated mesopores in Fig. 17 do not appear to influence the surface properties of the direct-write film, suggesting that the volume of gases evolved by isolated mesopores was not sufficient to cause large disruptions of the film surface that would lead to pit formation.

From the TEM and AFM results, it is clear that pores are not uniformly distributed within the irradiated films, and at the local level there are large variations in both pore sizes and levels of porosity arising from the inhomogeneity within the structure of the direct-written film. This is problematic since any functionality influenced by porosity (optical, dielectric, and mechanical properties) is non-uniform in nature even within blanket exposed films and thus observations based on bulk material characteristics are only crude estimates of the true characteristics of regions within these films. Since the quantitative values of induced porosity calculated using Lorentz–Lorenz and Maxwell–Garnett mixing rules assumed that air was well mixed with the matrix within the films (*i.e.* film homogeneity), they only provide estimates of the average properties of the films and are not strictly valid for determining actual levels of porosity at specific locations. Scattering induced by the surface roughness also adversely affected the refractive index measurements to a greater extent than the dielectric constant readings hence the porosities estimated by using dielectric constant values are more reliable than those estimated by the refractive index values. However, the porosities estimated by refractive index and dielectric constant mixing rules are in close agreement and they are comparable to those reported in the literature for similar sacrificial polymer loadings.[2–4,7,28,29]

By using photomasks with feature linewidths ranging from <10 μm to >100 μm, the feature resolution of the direct-write technique was tested for contact exposure applications. We

observed that although the direct-write process shown in Fig. 4 allowed patterning of arbitrary shapes and complex designs, the direct-written features had indistinct core/cladding boundaries. By comparing the dimensions of indistinct features as processing parameters such as PEB temperature and time were varied, we concluded that the fuzzy boundaries were a result of acid diffusion that arose from the formation of an acid concentration gradient within the film after UV exposure. The acid gradient was produced because acid was only formed in irradiated areas, while no acid was initially present underneath opaque areas of the photomasks.[73] As acid molecules diffused from exposed to unexposed areas across the core/cladding boundary, partial decomposition of PNC occurred in the unexposed region adjacent to the boundary. The final result of the acid diffusion was image spreading of the photoactive region, which is a common limitation of the linewidth resolution of resists.[74–77] The diffusion of photogenerated acid into unexposed regions also led a decrease of the waveguide core linewidth owing to decomposition of PNC as acid molecules permeated the core/cladding boundary. Preliminary studies have shown that, depending on PEB conditions, patterned core linewidths varied from being between 3 μm and 17 μm thinner than the width of the opaque lines on the photomask thus limiting the fine-feature patterning capability of the direct-write process to features with dimensions measuring several microns.

One method for reducing the image spreading of the photogenerated acid in the direct-write system is to increase the ratio of PBG to PAG prior to spin-coating the wafer.[76] In such a system photogenerated bases would neutralize acid molecules that diffuse into the unexposed regions thus quenching acid diffusion and decreasing the diffusion length.[76] Further studies need to be performed to determine the optimal formulation and processing conditions for achieving minimal acid diffusion and highest resolution of core and cladding features. In light of the diffusion of photogenerated acid into core regions, it is expected that the direct-write method outlined in this paper leads to graded profiles of porosity and refractive index and thus the core/cladding Δ(refractive index) shown in Fig. 14 is the maximum difference between core and cladding regions of an A-type direct-write film.

Conclusions

A processing technique was presented in which UV exposure was used to create both blanket porosity and laterally patterned porosity within dielectric films. This process relied on the ability of photogenerated acids to cause main chain scission and volatilization of polycarbonate-based sacrificial polymers templated in a crosslinkable dielectric matrix. The results were repeatable and processing was performed in a laboratory using commercially available materials and low-cost equipment. The average level of induced porosity scaled with the initial sacrificial polymer loadings but direct-written pores were unevenly distributed within the films and the microstructures were non-homogeneous. For optimal conditions, direct-written films with sacrificial polymer loadings of 20 wt% with respect to matrix solids produced roughly an average of porosity of 21 vol% to give a final interline dielectric constant of 2.36, and a refractive index value of 1.313. Both elongated mesopores (measuring 10 nm by about 20–30 nm), and elongated macropores (measuring 100 nm by about 200 nm) were produced within the internal structure of direct-written films. It is believed that the mesopores were a direct result of the decomposition of the photodefinable polymer whereas the macropores were likely a result of coalescence of the mesopores due to film shrinkage.

Acknowledgements

The authors would like to acknowledge the sample donations of research-grade PNC and FOx®-1x resins by Promerus LLC and Dow Corning Corp., respectively. The *N*-methylnifidepine PBG was synthesized, purified and its structure, **4**, verified using ^{1}H-NMR by Takashi Okada, a visiting scientist from JSR. The authors would also like to thank Professor Seth Marder in the Department of Chemistry at the Georgia Institute of Technology for offering advice regarding PBG synthesis. Thin TEM sections were prepared by Martin Brucherseifer using the facilities in the FIB2 Center at the Georgia Institute of Technology established under NSF : CRIF project # 0343028. TEM analyses were performed by Yolande Berta using the facilities in the Center of Nanostructure Characterization and Fabrication at the Georgia Institute of Technology. AFM analyses were performed by Dhananjay Bhusari using the facilities located in the Microelectronics Research Center located at the Georgia Institute of Technology. This material is based on work supported by the STC program of the National Science Foundation under agreement # DMR-0120967.

References

1 K. Maex, M. R. Baklanov, D. Shamiryan, F. Iacopi, S. H. Brongersma and Z. S. Yanovitskaya, *J. Appl. Phys.*, 2003, **93**, 8793–8841.
2 J. L. Hedrick, R. D. Miller, C. J. Hawker, K. R. Carter, W. Volksen, D. Y. Yoon and M. Trollsas, *Adv. Mater.*, 1998, **10**, 1049–1053.
3 K. R. Carter, R. A. DiPietro, M. I. Sanchez and S. A. Swanson, *Chem. Mater.*, 2001, **13**, 213–221.
4 J. W. Labadie, J. L. Hedrick, V. Wakharkar, D. C. Hofer and T. P. Russell, *IEEE Trans. Compon., Hybrids, Manuf. Technol.*, 1992, **15**, 925–930.
5 A. M. Padovani, S. A. Bidstrup Allen and P. A. Kohl, *Proceedings of 8th International Advanced Packaging Materials Symposium*, Stone Mountain, GA, USA, 2002, ed. R. Tummala, IEEE, Piscataway, NJ, USA, 2002, pp. 20–24.
6 A. M. Padovani, L. Rhodes, S. A. Bidstrup Allen and P. A. Kohl, *J. Electrochem. Soc.*, 2002, **149**, 161–170.
7 A. M. Padovani, L. Riester, L. Rhodes, S. A. Bidstrup Allen and P. A. Kohl, *J. Electrochem. Soc.*, 2002, **149**, 171–180.
8 A. M. Padovani, L. Rhodes, L. Riester, G. Lohman, B. Tsuie, J. Conner, S. A. Bidstrup and P. A. Kohl, *Electrochem. Solid-State Lett.*, 2001, **4**, 25–28.
9 H.-J. Lee, E. K. Lin, H. Wang, W. Wen-li, C. Wei and E. S. Moyer, *Chem. Mater.*, 2002, **14**, 1845–1852.
10 F. Iacopi, M. R. Baklanov, E. Sleeckx, T. Conard, H. Bender, H. Meynen and K. Maex, *J. Vac. Sci. Technol., B*, 2002, **20**, 109–115.
11 B. Zhong, H. Meynen, F. Iocopi, K. Weidner, S. Mailhouitre, E. Moyer, C. Bargeron, P. Schalk, A. Peck, M. V. Hove and K. Maex, *Mater. Res. Soc. Symp. Proc.*, 2002, **716**, 575–580.
12 F. Iacopi, Z. Tokei, Q. T. Le, D. Shamiryan, T. Conard, B. Brijs, U. Kreissig, M. Van Hove and K. Maex, *J. Appl. Phys.*, 2002, **92**, 1548.

13 V. Jousseaume, M. Fayolle, C. Guedj, P. H. Haumesser, C. Huguet, F. Pierre, R. Pantel, H. Feldis and G. Passemard, *J. Electrochem. Soc.*, 2005, **152**, 156–161.
14 P. De Rouffignac, Z. Li and R. G. Gordon, *Electrochem. Solid-State Lett.*, 2004, **7**, 306–308.
15 B. P. Gorman, D. W. Mueller, O. Chyan and R. F. Reidy, *Advanced Metallization Conference 2005 (AMC 2005)*, Colorado Springs, CO, United States, 2006, ed. S. H. Brongersma, T. C. Taylor, M. Tsujimura and K. Masu, MRS, Warrendale, PA, USA, 2006, pp. 392–397.
16 M. R. Baklanov and K. P. Mogilnikov, *Microelectron. Eng.*, 2002, **64**, 335–349.
17 M. R. Baklanov, E. Kondoh, E. K. Lin, D. W. Gidley, H. J. Lee, K. P. Mogilnikov and J. N. Sun, *Proceedings of the IEEE 2001 International Interconnect Technology Conference*, Burlingame, CA, USA, 2001, IEEE, Piscataway, NJ, USA, 2001, pp. 189–191.
18 J. H. Wang, W. J. Chen, T. C. Chang, P. T. Liu, S. L. Cheng, J. Y. Lin and L. J. Chen, *J. Electrochem. Soc.*, 2003, **150**, 141–146.
19 J.-N. Sun, Y. Hu, W. E. Frieze, W. Chen and D. W. Gidley, *J. Electrochem. Soc.*, 2003, **150**, 97–101.
20 Y. Xu, D. W. Zheng, Y. Tsai, K. N. Tu, B. Zhao, Q. Z. Liu, M. Brongo, C. W. Ong, C. L. Choy, G. T. T. Sheng and C. H. Tung, *J. Electron. Mater.*, 2001, **30**, 309–313.
21 J.-H. Yim, M. R. Baklanov, D. W. Gidley, H. Peng, H.-D. Jeong and L. S. Pu, *J. Phys. Chem. B*, 2004, **108**, 8953–8959.
22 C. Murray, C. Flannery, I. Streiter, S. E. Schulz, M. R. Baklanov, K. P. Mogilnikov, C. Himcinschi, M. Friedrich, D. R. T. Zahn and T. Gessner, *Microelectron. Eng.*, 2002, **60**, 133–141.
23 F. Iacopi, R. A. Donaton, B. Coenegrachts, T. Komiya, H. Struyf, M. Lepage, J. Van Aelst, W. Boullart, D. De Roest, I. Vos, M. R. Baklanov, G. Vereecke, M. Van Hove, M. Stucchi, Z. Tokei, H. Meynen, J. N. Bremmer, S. Vanhaelemeersch and K. Maex, *Proceeding of Advanced Metallization Conference (AMC)*, held October 2–5 in San Diego, CA, United States and October 19–20 in Tokyo, Japan, 2000, ed. D. Edelstein, G. Dixit, Y. Yasuda and T. Ohba, MRS, Warrendale, PA, USA, 2000, pp. 287–293.
24 R. K. Nahar, *J. Vac. Sci. Technol., B*, 2002, **20**, 382–385.
25 N. Nagayama, M. Shimono, T. Sato and M. Yokoyama, *Mol. Cryst. Liq. Cryst. Sci. Technol., Sect. A*, 2000, **349**, 119–122.
26 K. Tamaki, H. Takase, Y. Eriyama and T. Ukachi, *J. Photopolym. Sci. Technol.*, 2003, **16**, 639–648.
27 R. D. Miller and J. Michl, *Chem. Rev.*, 1989, **89**, 1359–1410.
28 S. Mimura, H. Naito, Y. Kanemitsu, K. Matsukawa and H. Inoue, *J. Organomet. Chem.*, 2000, **611**, 40–44.
29 S. Miura, A. Kobayashi, H. Naito, Y. Matsuura, K. Matsukawa and H. Inoue, *Synth. Met.*, 2003, **137**, 1405–1406.
30 Y. Nakayama, T. Kurando, H. Hayashi, K. Oka and T. Dohmaru, *J. Non-Cryst. Solids*, 1996, **198–200**, 657–660.
31 A. Watanabe, O. Ito, M. Matsuda, M. Suezawa and K. Sumino, *Jpn. J. Appl. Phys., Part 1*, 1994, **33**, 4133–4134.
32 A. Watanabe and M. Matsuda, *Macromolecules*, 1992, **25**, 484–488.
33 K. Matsukawa, S. Fukui, N. Higashi, M. Niwa and H. Inoue, *Chem. Lett.*, 1999, 1073–1074.
34 K. Matsukawa, K. Katada, N. Nishioka, Y. Matsuura and H. Inoue, *J. Photopolym. Sci. Technol.*, 2004, **17**, 51–52.
35 K. Matsukawa and Y. Matsuura, *Mater. Res. Soc. Symp. Proc.*, 2005, **847**, 45–56.
36 J. M. J. Frechet, F. Bouchard, E. Eichler, F. M. Houlihan, T. Iizawa, B. Kryczka and C. G. Willson, *Polym. J.*, 1987, **19**, 31–49.
37 J. P. Jayachandran, H. A. Reed, H. Zhen, L. F. Rhodes, C. L. Henderson, S. A. Bidstrup and P. A. Kohl, *J. Microelectromech. Syst.*, 2003, **12**, 147–159.
38 J. V. Crivello, *Chemistry of photoacid generating compounds*, ACS, Washington DC, USA, 1989.
39 J. V. Crivello, *J. Polym. Sci., Part A: Polym. Chem.*, 1999, **37**, 4241–4254.
40 J. V. Crivello and S. Kong, *Macromolecules*, 2000, **33**, 833–842.
41 J. V. Crivello and J. H. W. Lam, *J. Polym. Sci., Polym. Symp.*, 1977, 383–395.
42 J. V. Crivello and J. H. W. Lam, *J. Polym. Sci., Polym. Lett. Ed.*, 1978, **16**, 563–571.
43 J. V. Crivello and J. L. Lee, *Polym. Photochem.*, 1982, **2**, 219–226.
44 J. V. Crivello, J. Ma and F. Jiang, *J. Polym. Sci., Part A: Polym. Chem.*, 2002, **40**, 3465–3480.
45 J. P. Fouassier, D. Burr and J. V. Crivello, *J. Macromol. Sci., Pure Appl. Chem.*, 1994, **A31**, 677–701.
46 M. Shirai, K. Suyama, H. Okamura and M. Tsunooka, *J. Photopolym. Sci. Technol.*, 2002, **15**, 715–730.
47 M. Shirai and M. Tsunooka, *Prog. Polym. Sci.*, 1996, **21**, 1–45.
48 S. Tagawa, S. Nagahara, T. Iwamoto, M. Wakita, T. Kozawa, Y. Yamamoto, D. Werst and A. D. Trifunac, *Proc. SPIE–Int. Soc. Opt. Eng.*, 2000, **3999**, 204–213.
49 J. L. Dektar and N. P. Hacker, *J. Am. Chem. Soc.*, 1990, **112**, 6004–6015.
50 J. F. Cameron, C. Grant Willson and J. M. J. Frechet, *J. Am. Chem. Soc.*, 1997, **118**, 12925–12937.
51 A. M. Sarker, A. Lungu, A. Mejiritski, Y. Kaneko and D. C. Neckers, *J. Chem. Soc., Perkin Trans. 2*, 1998, 2315–2331.
52 G. A. Epling and M. E. Walker, *Tetrahedron Lett.*, 1982, **23**, 3843–3846.
53 S. Matuszczak, J. F. Cameron, J. M. J. Frechet and C. G. Wilson, *J. Mater. Chem.*, 1991, **1**, 1045–1050.
54 M. Tsunooka, H. Tachi, T. Yamamoto and M. Shirai, *Polym. Prepr. (Am. Chem. Soc., Div. Polym. Chem.)*, 2001, **42**, 720–721.
55 C. G. Willson, J. F. Cameron and J. M. J. Frechet, *Polym. Mater.: Sci. Eng.*, 1996, **74**, 437.
56 M. R. a. Winkle and K. A. Graziano, *J. Photopolym. Sci. Technol.*, 1990, **3**, 419–422.
57 B. R. Harkness, K. Takeuchi and M. Tachikawa, *Macromolecules*, 1998, **31**, 4798–4805.
58 B. R. Harkness, K. Takeuchi and M. Tachikawa, *Polym. Adv. Technol.*, 1999, **10**, 669–677.
59 Y. K. Siew, G. Sarkar, X. Hu, J. Hui, A. See and C. T. Chua, *J. Electrochem. Soc.*, 2000, **147**, 335–339.
60 W. C. Oliver and G. M. Pharr, *J. Mater. Res.*, 1992, **7**, 1564–1580.
61 H.-C. Liou and J. Pretzer, *Thin Solid Films*, 1998, **335**, 186–191.
62 W.-C. Liu, C.-C. Yang, W.-C. Chen, B.-T. Dai and M.-S. Tsai, *J. Non-Cryst. Solids*, 2002, **311**, 233–240.
63 J. N. Bremmer, Y. Liu, K. G. Gruszynski and F. C. Dall, *Mater. Res. Soc. Symp. Proc.*, 1997, **476**, 37–44.
64 C.-C. Yang and W.-C. Chen, *J. Mater. Chem.*, 2002, **12**, 1138–1141.
65 M. A. Brook, *Silicon in Organic, Organometallic, and Polymer Chemistry*, John Wiley & Sons, New York, 2000.
66 L. H. Sommer, *Stereochemistry, mechanism and silicon; an introduction to the dynamic stereochemistry and reaction mechanisms of silicon centers*, McGraw-Hill, New York, 1965.
67 R. West, *J. Am. Chem. Soc.*, 1954, **76**, 6015–6017.
68 K. J. Shea and D. A. Loy, *Acc. Chem. Res.*, 2001, **34**, 707–716.
69 Y. Toivola, J. Thurn and R. F. Cook, *J. Electrochem. Soc.*, 2002, **149**, 9–17.
70 J. F. Cameron and J. M. J. Frechet, *J. Am. Chem. Soc.*, 1991, **113**, 4303–4313.
71 S. K. Lee, B.-J. Jung, T. Ahn, I. Song and H.-K. Shim, *Macromolecules*, 2003, **36**, 9252–9256.
72 Y. Matsuura, S. Miura, H. Naito, H. Inoue and K. Matsukawa, *J. Photopolym. Sci. Technol.*, 2002, **15**, 761–764.
73 A. L. Hines, Maddox and N. Robert, *Mass transfer: fundamentals and applications*, Prentice-Hall, Englewood Cliffs, NJ, 1985.
74 F. A. Houle, W. D. Hinsberg, M. Morrison, M. I. Sanchez, G. Wallraff, C. Larson and J. Hoffnagle, *J. Vac. Sci. Technol., B*, 2000, **18**, 1874–1885.
75 T. Itani, H. Yoshino, S. Hashimoto, M. Yamana, N. Samoto and K. Kasama, *Microelectron. Eng.*, 1997, **35**, 149–152.
76 T. Itani, H. Yoshino, S. Hashimoto, M. Yamana, N. Samoto and K. Kasama, *Polym. Mater. Sci. Eng.*, 1997, **77**, 432–433.
77 E. Richter, S. Hien and M. Sebald, *Microelectron. Eng.*, 2000, **53**, 479–483.